euspen's 21st International Conference & Exhibition, Copenhagen, DK, June 2021
www.euspen.eu

Design and optimization of a novel 2-DOF synchronous linear rotary drive

Berend Denkena, Benjamin Bergmann, Patrick Ahlborn*, Jonathan Fuchs

Institute of Production Engineering and Machine Tools (IFW), Leibniz University Hanover

**ahlborn@ifw.uni-hannover.de*

Abstract
Achieving movements of machine tool components in 2 degrees of freedom (DOF) usually requires a serial arrangement of at least two drives. The serial kinematic reduces the stiffness at the tool center point (TCP) and leads to an accumulation of the positioning and measuring errors of each drive. To achieve a high level of precision, a novel 2-DOF drive without serial kinematics is being developed. The drive consists of a static primary part and a secondary part with a linear and a rotary DOF. The secondary part is able to move in both DOFs independently. For this purpose, two separate windings which generate rotation and translation forces are stacked in the primary part. To generate magnetic forces in both DOFs, the secondary part is equipped with a checkerboard-like array of permanent magnets. The coupling between both windings and thus the induction of forces can be bypassed. This means that the windings can be controlled independently. The combination of the primary and secondary parts reduces the drive length. In comparison to current linear rotary drives, the novel drive is more compact and has a higher performance. In this paper, the motor geometry is optimized by parametric FEM-simulations. The goal of said optimization is to improve the torque and feed force as well as to reduce power losses and disturbing forces. For this purpose, a parametric model of the drive is developed. The simulations are carried out in ANSYS Maxwell and are run in 2D to save computing time. A genetic algorithm and sequential nonlinear programming are used to optimize the magnet height, pole-to-pole coverage, tooth angle and slot height. The simplifying assumptions of the 2D-simulation are compared to an additionally performed 3D-simulation. The result is an optimized drive with 8% higher performance and 65% less power loss compared to the non-optimized initial geometry.

Direct Drive, Linear Rotary Drive, Genetic Algorithm, Sequential Nonlinear Programming, Machine Tools

1. Introduction

The performance of feed drives has a significant impact on the precision and productivity of machine tools. A higher precision can be achieved by 2-degrees of freedom (DOF) drives due to the loss of the serial arrangement of at least two axes. Via the loss of the serial kinematics and thus the elimination of coupling elements, a higher stiffness of multi-DOF drives is realized. Therefore, the positioning and measuring errors of the individual axes do not accumulate due to the omission of the serial arrangement. On the other hand, the performance of 2-DOF drives is lower than in a serial arrangement and needs to be enhanced to establish 2-DOF drives. The performance of the drive is determined by the torque and force as well as by the amount of the disturbing cogging torque and force.

Only a few approaches to linear rotary 2-DOF drives have been successfully implemented at this point in time. The 2-DOF drives presented in [1] and [2] are based on a serial arrangement of two static primary parts along the drive axis. Both primary parts are used separately for force generation, whereby one primary part generates forces in the direction of rotation and the other primary part in the direction of translation. The performance is limited due to the lack of stator teeth between the coils. The authors of [3] and [4] use two static primary parts which are aligned along the radial axis of the drive. The inner stator is positioned inside of the hollow secondary part and is used for generating forces in the direction of rotation. The second stator is positioned outside of the secondary part and is used for force generation in the translation direction. The radial separation of the primary and secondary parts leads to a large required radial space. The small magnet height of the secondary part also reduces the performance. The drive in [5] consists of a primary part which is split into two halves along the drive axis. Each half of the primary part is designed for force generation in one DOF. Since the volume of primary parts per DOF is reduced by half, the performance is significantly lower. Another approach is described in [6] and [7] in which a helical, cross-shaped arrangement of coils is used. The approach is designed without stator slots which reduces the maximum performance. In addition, the rotation and translation movements cannot be controlled independently. For the drive of [8], a primary part with a radial arrangement of stacked windings is used. The inner stator is used for rotation- and the outer stator for translation movement. However, single layer windings are used which results in a lower magnetic flux. In addition to the performance, the positioning accuracy of a linear rotary drive is important. It is affected by the guideway. An air or roller bearing is used for all drives presented.

The aforementioned drives are not suitable for high performance applications due to their low performance. The lower performance is caused due to the basic design of the drives, e.g. the lack of stator teeth in some approaches. In addition to that, the guideway of the drives is inadequate for high performance and working loads. For this reason, the design of a new 2-DOF linear rotary drive is presented in this paper. The drive is designed for the application in lathe-milling centers. It is illustrated how the performance and power loss of the drive can be improved by FEM-optimization for higher performance. By this, optimization potentials are identified during the design process. In comparison to current approaches, the new drive has a higher performance and a hydrostatic guideway is used (Fig. 1 left). Hydrostatic guideways are often used for high precision manufacturing due to the absence of sliding friction caused by

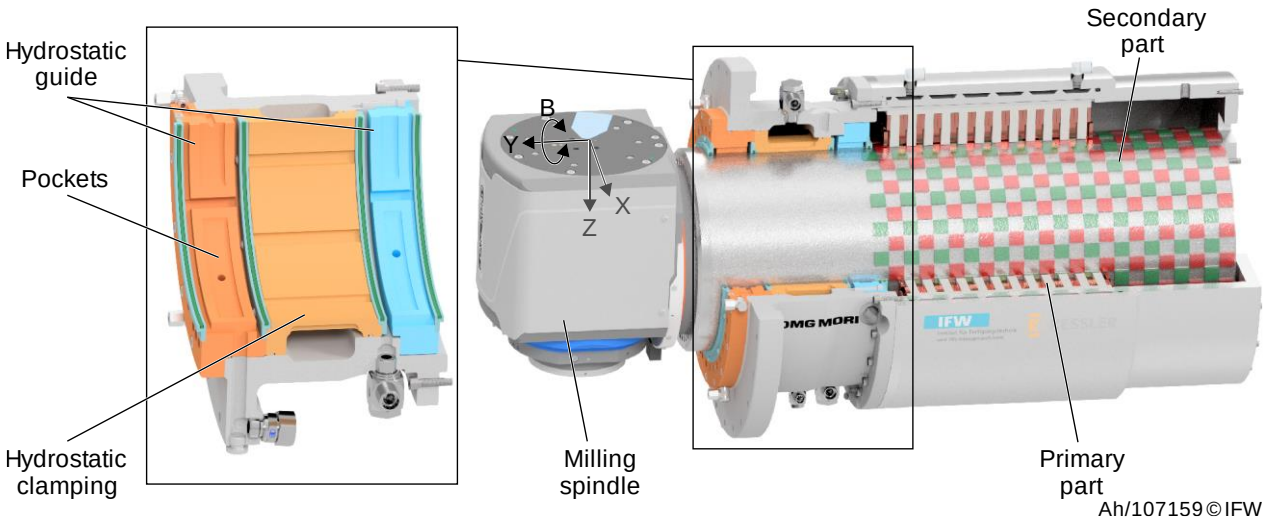

Figure 1. Drive design of the 2-DOF linear rotary drive with hydrostatic guideway and clamping system as well as a milling spindle

lubricating oil. Thus, there is no danger of the stick-slip effect and a higher stiffness can be achieved. Therefore, the basic design of the drive is described in section 2. The presented drive geometry is then optimized by a genetic algorithm (GA) and sequential nonlinear programming (SNLP) which is shown in section 3. The optimized drive design is analyzed in terms of the performance using the 2D simulations which are presented in section 4. By performing an additional 3D simulation, the simplifying assumptions of the 2D simulations were examined.

2. Drive design

The novel 2-DOF linear rotary drive is based on a 3-phase permanent magnet synchronous drive. The design of the entire drive module is shown in Fig. 1. It consists of a static primary part and a secondary part with a linear and a rotary DOF. For the application in lathe-milling centers, a milling spindle can be attached to the secondary part of the drive. The drive module is equipped with a hydrostatic guideway and a clamping element for high-precision applications at high loads.

The hydrostatic guideway system is used to allow a high level of precision while positioning and was designed to absorb a torque of approx. 3,000 Nm and forces of approx. 20,000 N. This is achieved by integrating an additional hydrostatic clamping element. The clamping element can lock the secondary part at high loads to prevent a deflection of the secondary part and thus of the tool center point (TCP) as well. The designed stiffness of the hydrostatic guideway system is 249 N/µm.

In Fig. 2, a parametric model of the drive design is shown. The secondary part is able to move in both DOFs along the Y- and B-axis independently. For this purpose, a cross winding system is established. The cross winding scheme consists of two separate concentrated windings which are arranged at 90° on top of each other in the primary part, generating rotation and translation forces. The inductive coupling between both windings and thus the induction of forces can be bypassed by setting the same winding number for both DOFs [9]. As result, both windings can be controlled by standard frequency converters for 1-DOF drives. The primary part is designed with stator teeth to improve the magnetic flux. To generate magnetic forces in both DOFs, the secondary part is equipped with a checkerboard-like array of neodymium iron boron permanent magnets. The design of the magnet array is similar to the one described in [7]. The drive design is then optimized by using the FEM to improve performance.

3. Motor optimization

The parametric model of the drive is the basis of the FEM optimization. Parameters of the model which can be varied in the simulation are the magnet height h_{PM}, pole-to-pole coverage of the magnets α, tooth angle α_T, and the slot height h_S in the rotary direction. The tooth angle defines the opening angle of the stator teeth and thus the teeth width. The applied stator material is non grain oriented electrical metal sheet M330-35A. The adjustable model parameters (marked with an asterisk) as well as the framework parameters, which are determined based on an analytical pre-dimensioning, are shown in Table 1.

Table 1 Initial drive values.

Parameter	Value
Number of slots N1 (-)	36
Number of pole pairs 2p (-)	42
Stator diameter d (mm)	360
Air gap width δ (mm)	1
Stator length l (mm)	315
Magnet height h_{PM} (mm) *	4
Pole-to-pole coverage α (%) *	0.85
Tooth angle α_T (°) *	2.5
Slot height h_S (mm) *	10

The optimization is carried out in ANSYS Maxwell. To achieve a high model accuracy, the simulation was implemented as a magnetic transient simulation. This allowed to consider nonlinear effects. In order to reduce the calculation time, the optimization is performed in a 2D section of the rotary plane of the drive. The 2D rotation model length $l_{model,2D}$ is a scaling factor which is used to scale the simulation results of the 2D rotation section to an equivalent of the real drive length l_{real} and is calculated by Eq. 1.

$$l_{\mathrm{model,2D}} = k \cdot l_{\mathrm{real}} \tag{1}$$

The geometric factor of k is 0.37 and was determined in previous work. The mesh size of the FEM model was selected individually for each part of the drive. The air gap, for example, has the smallest element size (0.5 mm), as it has the lowest magnetic permeability and it is the area where the forces are generated. Through preliminary examinations, the mesh quality was successfully assigned by taking into account different mesh sizes to reproduce the cogging torque in the simulations, since this

requires a fine mesh. For the optimization, a cost function can be established as seen in the following Eq. 2.

$$c(\varepsilon) = \sum_{1}^{N} w_i \cdot \varepsilon_j^2 \qquad (2)$$

Equation 2 is based on the Euclidean norm. The error ε of each individual optimization goal g(i) and is weighted with the weight w. The total number of optimization goals is described by N. The individual goals i are defined by using a logical sentence shown in Eq. (3).

$$g(i) = calculation_{(i)} \cdot condition_{(i)} \cdot goal_{(i)} \cdot weighting_{(i)} \qquad (3)$$

Three individual goals are set up for the drive optimization and are all equally weighted (Table 2). The goals correspond to the to target parameters of the drive performance to be optimized.

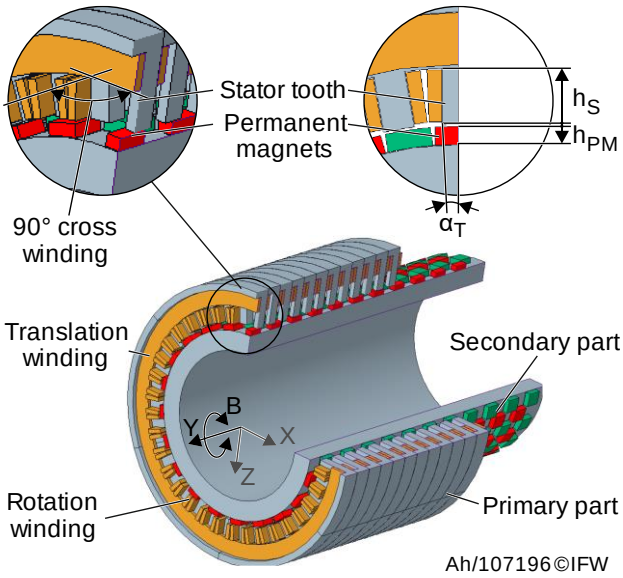

Figure 2. Parametric drive model for FEM optimization

Table 2 Optimization goals for cost function

Calculation	Condition	Goal	Weighting
Torque	≥	1,000 Nm	1
Cogging torque	≤	3% of average torque	1
Power loss	≤	1,000 W	1

The cost function is minimized by using a genetic algorithm and a sequential nonlinear programming. These two optimizers are used to get a wider variety of drive geometry candidates and are described in the following. The GA is a stochastic optimizer. Thus, the cost function is used to show the compliance with the optimization goals but not to determine the design parameters. Instead, a selection of randomly chosen design parameters is applied to the model parameters in a structured manner to create new drive geometries. In this way, in each iteration, a defined quantity of new individual drive geometries can be created while a defined amount of old geometries are discarded. During this procedure, the drive geometries were simulated and rated with respect to the cost function. Highly rated geometries were preferred. It should be noted that local minima of the cost function are avoided due to the random selection of parameters by the GA. In contrast to the GA, the SNLP is a deterministic optimization algorithm. Thus, the FEM results are approximated by response surfaces. The response surfaces are Taylor series approximations, which are set up by the resulting simulation results. By calculating the gradients of the response surface in each optimization loop, the direction and distance of the next iteration step can be set by the algorithm. In addition, the response surfaces and the evaluation of the cost function can be used to estimate the design parameters to be improved.

Four optimization setups were carried out by varying the magnetomotive force in setup 1 and 2 boundaries values of 500 A and 1,500 A for GA and SNLP. In setups 3 and 4, the magnetomotive force for GA and SNLP is fixed to a value of 1,500 A. By implementing different ranges of the magnetomotive force, different boundary conditions for the optimization were set to obtain a greater variety of drive geometry candidates. During optimization, the SNLP converges (Fig. 3) whereas the GA has a stochastic variation in its residual due to its stochastic algorithm. Thus, the SNLP optimization stops after the 26th iteration because a minima is found. Nevertheless, the residual of the GA has stochastic local minima which can be identified. The generated geometry of SNLP in setup 2 after 26 iterations was best rated with respect to the optimization goals. Thus, in the following, only the SNLP-optimized geometry is examined. The model parameters in the direction of translation were set based on the model values in the direction of rotation. The results of the optimization are shown in section 4.

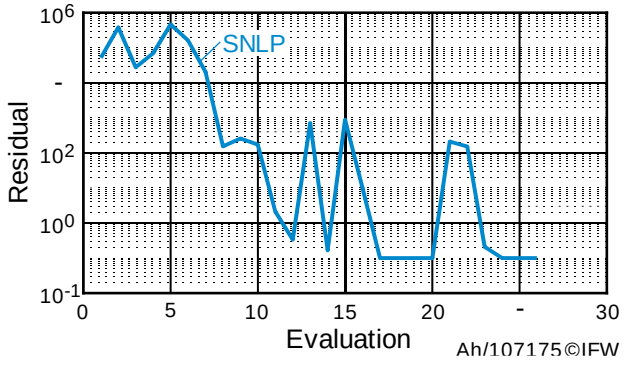

Figure 3. Residual of SNLP optimization in setup 2

4. Simulation results

The change of the SNLP-optimized model parameters with respect to the initial values is shown in Fig. 4. By SNLP optimization, all model parameter values are increased, whereby the magnet height and slot height were adjusted the most. The larger magnet height h_{PM} leads to a stronger magnetic flux and thus to higher torque and force. By increasing the slot height h_S, the power loss is reduced due to a lower current density as a result of a larger cross area. The force and disturbing forces are influenced by the pole coverage α, since the overlapping surface of the magnets with the stator teeth is affected. The area between two stator teeth and thus the winding area is defined by the tooth angle α_T. An increase of the tooth angle leads to higher force but also to a higher power loss due to the smaller winding area. By using the SNLP optimization, an optimum of the parameters can be found.

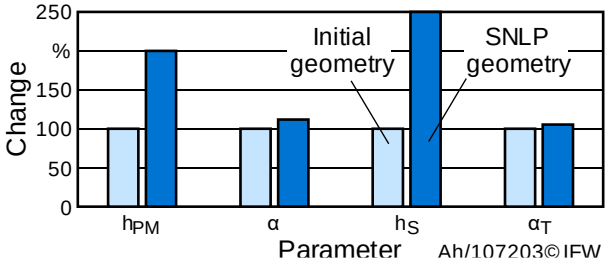

Figure 4. Change of SNLP-optimized model parameter

The optimized geometry generated by the SNLP has an 8% higher torque and 69% lower cogging torque compared to the initial geometry. The comparison between the initial geometry and SNLP geometry is shown in Fig. 5, in which β corresponds to the rotation angle of the B-axis. A periodic variation of the cogging torque is observed and results of the interaction of the stator teeth with the permanent magnets. The period of the cogging torque can be determined to 1.39 ± 0.0542° which corresponds well to the analytical calculation of 1.42°. The torque is lowered by cogging torque as well as other disturbing forces which results in a slightly periodic oscillation of the torque. In addition, the loss of the winding for rotation movement could be reduced by 65%, as the winding cross-area is larger due to larger slot height.

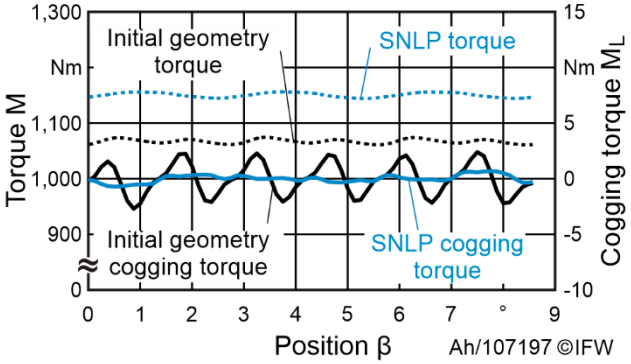

Figure 5. Torque and cogging torque of SNLP designed geometry in comparison to reference start geometry

In the 2D translation section simulation, a 6% higher feed force of the SNLP-optimized geometry can be observed. In addition, the cogging force increases by 175 % (Fig. 6). However, the increase of the cogging force is less than 6% of the maximum feed force and can be compensated by the control system. The movement along the Y-axis is indicated by the parameter y. In the period of the cogging force, a harmonic can be detected. This is caused by a disturbing force which results from the interaction of the outer stator teeth with the magnets. The loss in the translation windings is reduced by 58%. The simulated magnetic flux distribution is shown in Fig. 7. The average air gap flux is 1.1 ± 0.16 T. The teeth corners have a magnetic flux of 2.4 T, which is slightly above the saturation of electrical steel at 2 T. However, the oversaturation is only present in a small area at the teeth corners and at maximum magnetomotive force.

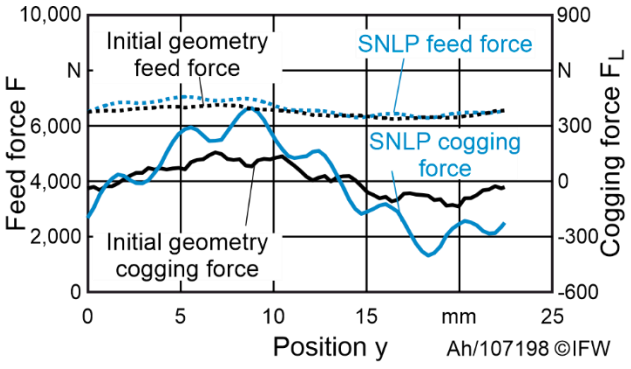

Figure 6. Feed force and cogging force of SNLP designed geometry in comparison to reference start geometry

In the 3D rotation simulation, results similar to the those of the 2D simulation could be determined. The maximum difference between both simulations was determined to be 3 %. Based on this congruency, it could inferred that the simplified assumptions of the 2D simulation, such as the scaling factor of the 2D model length, are accurate. Therefore, the used 2D model length is correct. However, an overall accuracy or uncertainty of the results cannot be given, since the simulations were used to optimize and set up the drive geometry. Finally, the drive geometry optimized through SNLP allows 1,154 Nm effective torque and 6,809 N force which is similar to 1-DOF drives. The power loss in the direction of translation is about 7,217 W and in rotation 5,252 W.

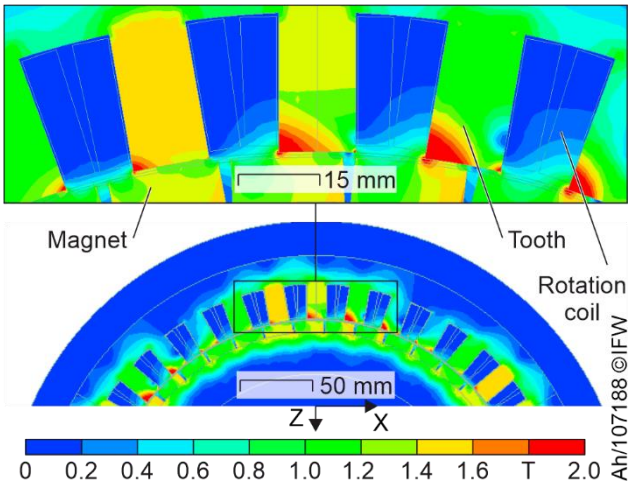

Figure 7. Flux distribution of SNLP designed geometry

5. Summary and conclusion

In this paper, a new 2-DOF drive design with high performance density and a precise hydrostatic guideway system is introduced. The new linear rotary actuator has a performance similar to that of a 1-DOF actuator, but can move in 2-DOF. The resulting elimination of the serial kinematics leads to a higher stiffness. Also, stator teeth with cross windings and a checkerboard-like array of permanent magnets are used for the new designed drive. It was possible to increase the drive performance by applying a geometric optimization based on a genetic algorithm and sequential nonlinear programming. As a result, the performance of the optimized drive is 8% higher and the power loss is reduced by 65% compared to the initial geometry of the designed drive.

In order to validate the simulation results, a drive based on the optimized geometry will be assembled in the future. Both the power and the power loss are then measured to determine the accuracy of the simulation. The stiffness and position error as well as the performance will then be compared with serial B-Y-axis kinematics of lathe-milling centers to examine the usability of the 2-DOF drive for machine tools.

References

[1] Meessen K, Paulides, J, Lomonova E 2011 *IEEE International Electric Machines & Drives Conference (IEMDC)* 336-241

[2] Overboom T, Jansen J, Lomonova E, Tacken F 2009 *IEEE International Electric Machines & Drives Conference* 1043-1050

[3] Xu L, Lin M, Fu X, Liu K, Guo B 2016 *IEEE Transactions on Magnetics* ***52*** 1-4

[4] Xu L, Lin M, Fu X, Liu K, Guo B 2017 *Energies* **10** 493

[5] Si J, Feng H, Ai L, Hu Y, Cao W 2015 *IEEE Transactions on Energy Conversion* **30** 1200-1208

[6] Tanaka S, Shimono T, Fujimoto Y 2014 *Proceedings, IECON 2014 - 40th Annual Conference of the IEEE Industrial Electronics Society* 508-513

[7] Tanaka S, Shimono T, Fujimoto Y 2015 *Proceedings - 2015 IEEE International Conference on Mechatronics* 529-534

[8] Chen L, Hofmann W 2007 *IEEE 7th International Conference on Power Electronics and Drive Systems* 1372-1376

[9] Denkena B, Friedrichs J, Fuchs J, 2015 *Production Engineering* **9** 125-132